Surface diffusion of CO on silica-supported Ru particles: ^{13}C nuclear magnetic resonance studies

T. M. Duncan and A. M. Thayer
AT&T Bell Laboratories, Murray Hill, New Jersey 07974

T. W. Root
University of Wisconsin, Madison, Wisconsin 53706

(Received 14 June 1989; accepted 7 November 1989)

Portions of CO adsorbed on Ru particles, selected by the orientation of the C–O bond relative to an external magnetic field, are labeled by inversion of the ^{13}C nuclear magnetic dipole. Changes in the orientation of the CO bond of these labeled molecules are then observed with ^{13}C NMR spectroscopy. The temperature dependence and rate of reorientation are consistent with surface diffusion on Ru particles with small numbers of flat faces. The insensitivity to CO pressure in the range 0.5–100 Torr discounts stimulated desorption by gas-phase CO.

I. INTRODUCTION

The reaction mechanism and reaction rate of CO adsorbed on oxide-supported transition-metal catalysts are related to its mobility and residence times. At reaction temperatures and pressures, relevant processes include desorption to (or exchange with) the gas phase, diffusion on the metal particles, and exchange between chemically inequivalent sites. The surface diffusion of CO on silica-supported Pd clusters has been measured by NMR line-shape analysis.[1] In this paper we apply NMR spin-population labeling techniques to probe the dynamics of CO on Ru particles, and thus determine which process dominates and measure its rate for the temperature range 298–375 K and pressure range 0.5–200 Torr.

NMR spin-labeling techniques for the study of dynamics at surfaces have been previously demonstrated in studies of formic acid on titania[2] and hydrogen on Rh particles.[3] In these studies the technique was used to label selectively one of two different species in each sample; physisorbed vs chemisorbed formic acid[2] and hydroxyls vs hydrogen on Rh.[3] In this present study of adsorbed CO we demonstrate different selectivity—the labeling of a subgroup of molecules that are chemically identical to the unlabeled molecules, but differ only by their spatial orientation.

The ^{13}C NMR spectra of CO on highly dispersed Ru can be decomposed into three components representing linearly bonded CO, bridge-bonded CO, and motionally averaged multicarbonyl sites.[4] Further refinements based on magic-angle spinning studies suggest that the linearly bonded CO may exist as two species.[5] Based on similarities to the spectra of CO on highly dispersed Rh, it is assumed that the linear- and bridge-bonded CO correspond to sites on Ru particles and the multicarbonyls are formed on isolated Ru atoms. Although the solid-state NMR spectra of these three components overlap, the motionally averaged component is a sharp line that spans a small frequency range near the center of mass. Thus, the behavior of CO on the Ru particles may be observed by labeling portions of the spectrum on either side of the center peak. The frequency shift from the center peak is determined by the CO orientation; the high-frequency limit corresponds to CO perpendicular to the external magnetic field and the low-frequency limit corresponds to CO parallel to it. Thus, one can selectively label a portion of the CO on the Ru particles, on the basis of the orientation of the CO bond, by inverting a portion of the ^{13}C NMR powder pattern. Any subsequent motion that changes the orientation of the CO bond of the labeled portion will be revealed by a change in the inversion profile in the powder pattern.

II. EXPERIMENTAL PROCEDURES

A. Catalyst samples

This study concerns the dynamics of adsorbed CO in three Ru/silica samples. The site distributions of adsorbed CO on each of these samples, as measured by ^{13}C NMR, were the subjects of previous studies.[4,6,7] For continuity, we retain the original sample labels: Ru/silica (B),[4] Ru/silica (E),[6] and Ru/silica (I).[7] Refinements to the initial analysis have subsequently been reported for Ru/silica sample (B).[5] The CO-to-metal ratios, CO pressures, CO distributions, and ^{13}C NMR parameters for the catalyst samples are given in Table I. The 2.5 wt % samples [(B) and (E)] were prepared by amine cation exchange and the 4.3 wt. % sample (I) was prepared by incipient wetness. Samples (B), (E), and (I) were 38, 5, and 31 months old, respectively, at the time they were examined for this study. Typical sample size was 0.3 g with 10 mL volume overhead. Owing to the CO pressures, the Ru surfaces in all the samples are saturated. NMR measurement at elevated temperatures increases the CO pressure in a sample, but the CO coverage on the Ru remains essentially saturated over the range studied here (up to 375 K).

B. NMR

The spin-labeling experiment, diagramed in Fig. 1, consists of three periods: selective inversion, recovery, and detection. During the first period, a portion of the ^{13}C nuclear dipoles are selectively inverted. One method of selective inversion uses a long, weak 180° pulse as described elsewhere.[2] Where used in this study, the 180° inversion pulse was 0.40 ms long (1.2 G), which resulted in a hole of half-width 1.0 kHz. An alternate method involves a multiple-pulse approx-

 0021-9606/90/042663-10$03.00

TABLE I. Descriptions of catalyst samples.

Sample	wt. % metal	CO-to-metal ratio	P_{CO} (Torr)[b]	^{13}C NMR parameters[a] (at 298 K)						Ref.
				Species	Fract[c]	$\langle\sigma\rangle$	δ	η	$\Delta\sigma$	
Ru/silica (B)	2.5	1.66	100	Linear (1)	0.32	192	269	0.04	7	4,5
				Linear (2)	0.28	181	246	0.10	6	
				Bridged	0.21	250	154	0.27	21	
				Multicarbonyl	0.18	199	0	0.0	14	
Ru/silica (E)	2.5	1.41	0.5	Linear (1)	0.23	193	259	0.06	5	6
				Linear (2)	0.38	183	234	0.06	12	
				Bridged	0.11	234	149	0.37	20	
				Multicarbonyl	0.25	199	0	0.0	22	
Ru/silica (I)	4.3	0.23	0.0[d]	Linear	0.34	191	262	0.02	44	7
				Bridged	0.53	247	143	0.28	60	
				Multicarbonyl	0.10	201	0	0.0	65	

[a] The isotropic shift $\langle\sigma\rangle$ is in ppm, relative to tetramethylsilane (TMS). The chemical shielding parameters are defined as follows: $\delta = \langle\sigma\rangle - \sigma_{33}$ and $\eta = (\sigma_{11} - \sigma_{22})/\delta$. $\Delta\sigma$ is the broadening convoluted into the powder pattern for linear and bridged species, or half-width at half-height of the Lorentzian multicarbonyl peaks.

[b] At 298 K. Being sealed samples, the pressure at higher temperatures is proportionately higher.

[c] A CO_2 peak at 124 ppm brings each total to 1.0.

[d] After exposure to 200 Torr CO for 5 min, the sample was purged with Ar then sealed under 760 Torr Ar.

imation to a Gaussian-shaped pulse.[8] This sequence was used for the majority of the analysis in this study; unless stated otherwise, this was the sequence used. The sequence, shown in Fig. 1, consists of a series of pulses with uniform rf amplitude, but with a Gaussian variation in durations, which provides a Gaussian inversion profile. Using the formalism discussed elsewhere,[8(b)] we designed a 24-pulse sequence such that the tip angles of the pulses comprising the first half of this centrosymmetric sequence are 1.0°–1.4°–2.2°–3.2°–4.4°–6.0°–7.8°–9.6°–11.7°–13.3°–14.3°–15.1°. The gap between each pulse was 30 μs, for a total sequence length of 0.78 ms, which causes an approximately Gaussian hole of half-width 0.85 kHz (11 ppm in this study) and the first node occurs at 26.6 kHz (355 ppm) from resonance. The sequence was verified experimentally with a ^{13}C-enriched sample of $BaCO_3$. To accommodate the time resolution required for the shortest pulses, the rf is attenuated to 5.2 G (i.e., a 90° pulse requires 45 μs). Note that this method, as with all labeling experiments, can provide meaningful results only for phenomena slower than the labeling process, which is 0.78 ms here. Compared to the weak 180° pulse used previously to label surface-adsorbed species,[2] the Gaussian sequence offers the advantage of a simple inversion profile which facilitates analysis, but carries the disadvantage of requiring a longer time to invert a profile of similar width.

The length of the recovery period (τ_{rec}) must always exceed two criteria: the response time for the amplifier gain (30 μs) and the T_2^* of the sample ($\sim$25 μs). The nuclear

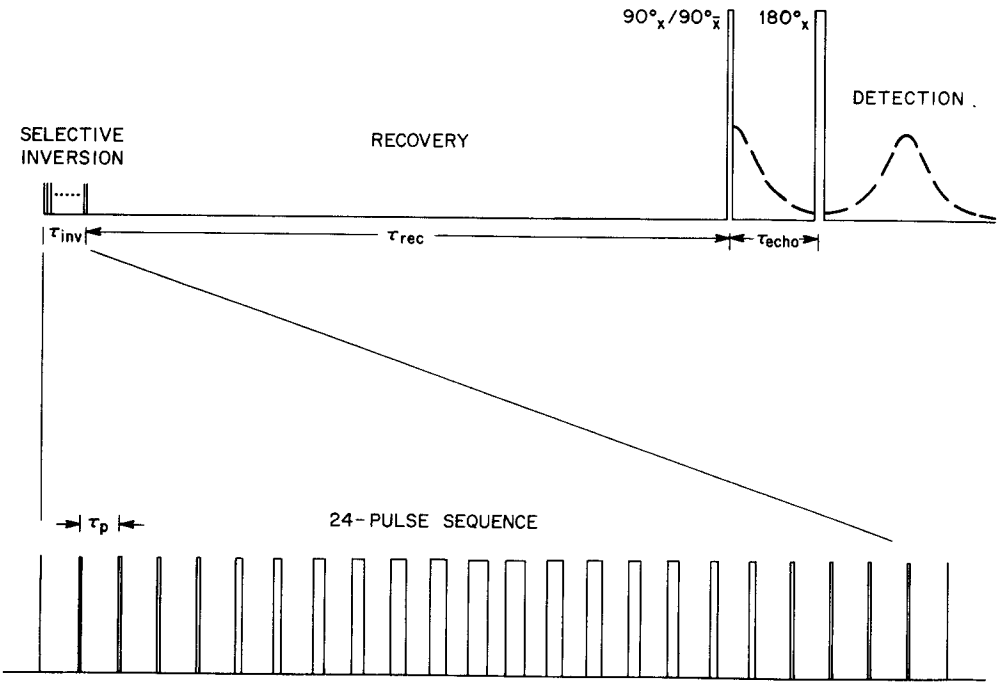

FIG. 1. A schematic diagram of the selective inversion experiment. Time periods are not drawn to scale; the inversion sequence spans 0.78 ms ($\tau_p = 30\mu$s), τ_{rec} ranges from 0.1 ms to 2.5 s, and τ_{echo} is 18 μs.

signal is detected as an echo from a "90°_x–180°_x-observe" sequence, with $\tau_{echo} = 18\ \mu s$. To reduce spectrometer recovery artifacts, on alternant scans a "$90^\circ_{\bar{x}}$–180°_x-observe" is used and the signals are subtracted. The 90°_x pulse length was $3.3\ \mu s$ (71 G).

NMR spectra were obtained on a Bruker CXP-200 console at a Larmor frequency of 75.434 MHz for ^{13}C. The temperature of the sample was controlled to $\pm 2\,^\circ$C by passing nitrogen through a Dewared sample volume. The NMR spectra are plotted on the δ scale for chemical shifts, relative to tetramethylsilane (TMS), with downfield signals being positive (i.e., C_6H_6 is at 128.7 ppm and CS_2 is at 192.8 ppm).

III. EXPERIMENTAL RESULTS

The motion of CO on the silica-supported Ru samples was probed by selectively inverting the ^{13}C nuclear dipoles of CO molecules oriented approximately perpendicular (80°) to the external magnetic field. The width of the hole corresponds to an angular half-width of 4°. The ^{13}C NMR spectra of Ru/silica (B) measured at various delays after a selective inversion pulse centered at 300 ppm are shown in Fig. 2 for 298 K, in Fig. 3 for 345 K, and in Fig. 4 for 375 K. Also included in each figure is a spectrum taken without selective inversion, for comparison. Each spectrum is the summation of 7000 scans taken at intervals of 6 s. Thus, the experiment shown in each figure requires ~80 h. It is noted that the spectrum of CO on Ru/silica changes with temperature. These changes, which are partially irreversible, are discussed elsewhere.[6]

The spectra for Ru/silica (E) at 298 K, in which the CO pressure is 200 times less than (B), are shown in Fig. 5. Each spectrum represented 30 000 scans taken at intervals of 4 s.

The spectra for Ru/silica (I) at 298 K, which is distinguished by low dispersion compared to (B) and (E), are shown in Fig. 6. The selective inversion in these spectra was caused by a weak 180° pulse. This inversion process is faster than the multiple-pulse Gaussian sequence (0.4 ms compared to 0.78 ms), which in part accounts for the more complete inversion; the T_2's of the CO on the particles are about 0.6 ms. When this weak 180° pulse was applied to sample B, the inversion was also essentially complete (not shown). However, both techniques are fast relative to the time constants of the motions studied here (see below). The Gaussian sequence is preferred because of the simpler shape. Unfortunately, this advantage is not obvious owing to the poor signal-to-noise levels in Fig. 6. Each spectrum represents 20 000 scans taken at intervals of 3 s. The add–subtract sequence used for detection[2] causes short-T_1 species, such as CO_2, to vanish from the spectrum at long times.

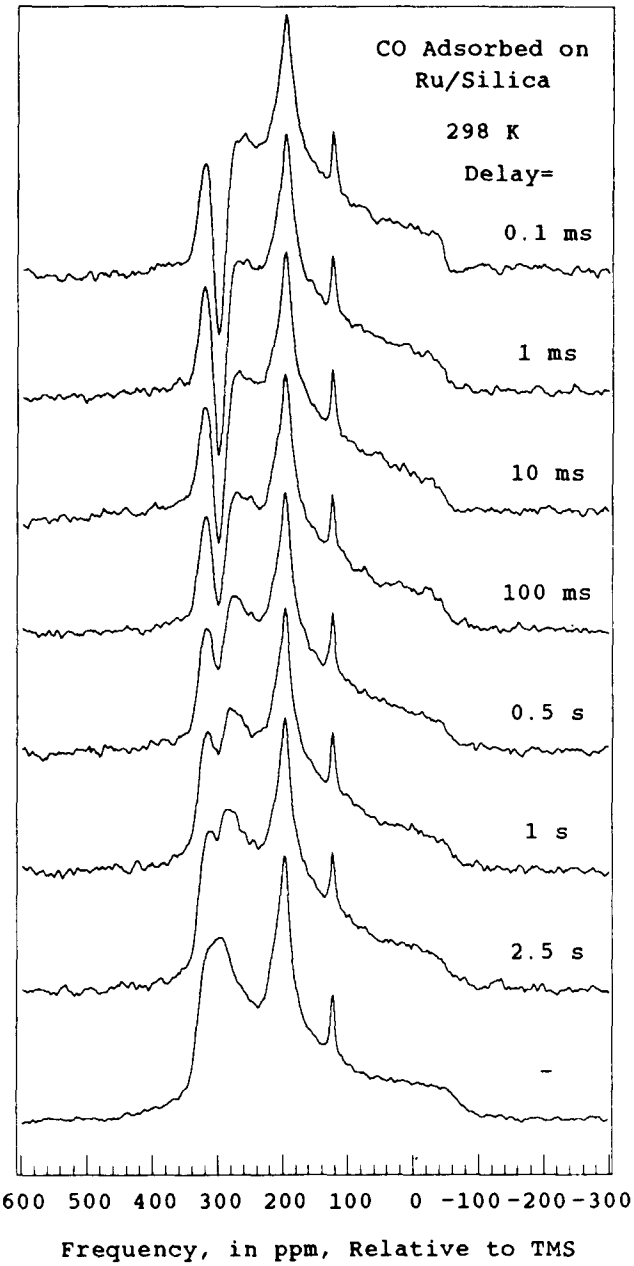

FIG. 2. ^{13}C NMR spectra of CO adsorbed on silica-supported Ru (B) at 298 K as a function of recovery time after selective inversion at 300 ppm. A spectrum measured without inversion is shown at the bottom.

IV. DISCUSSION OF RESULTS

A. Model for CO dynamics

The dynamics of the adsorbed CO are reflected by the evolution of the nonequilibrium magnetization created by the labeling pulse. Immediately after the system is labeled, the nonequilibrium magnetization has a profile whose position, amplitude, and width are determined by the pulse sequence. As the system evolves, the hole in the spectrum will recover. If there is no exchange or motion, the hole will recover by spin-lattice relaxation with time constant T_1. Motional processes with time constants shorter than T_1 will cause the hole to recover faster and (as will be shown) may cause characteristic changes in the shape of the nonequilibrium profile as well as the appearance of holes at other positions in the NMR spectrum. This section describes mathematical models for the evolution of selectively labeled NMR spectra of adsorbed CO.

The NMR spectrum at equilibrium (several T_1's after the labeling pulse) is the sum of several components, weighted by their relative abundances:

$$S(\omega,5T_1) = \sum_{i=1}^{n} w_i s_i(\omega). \tag{1}$$

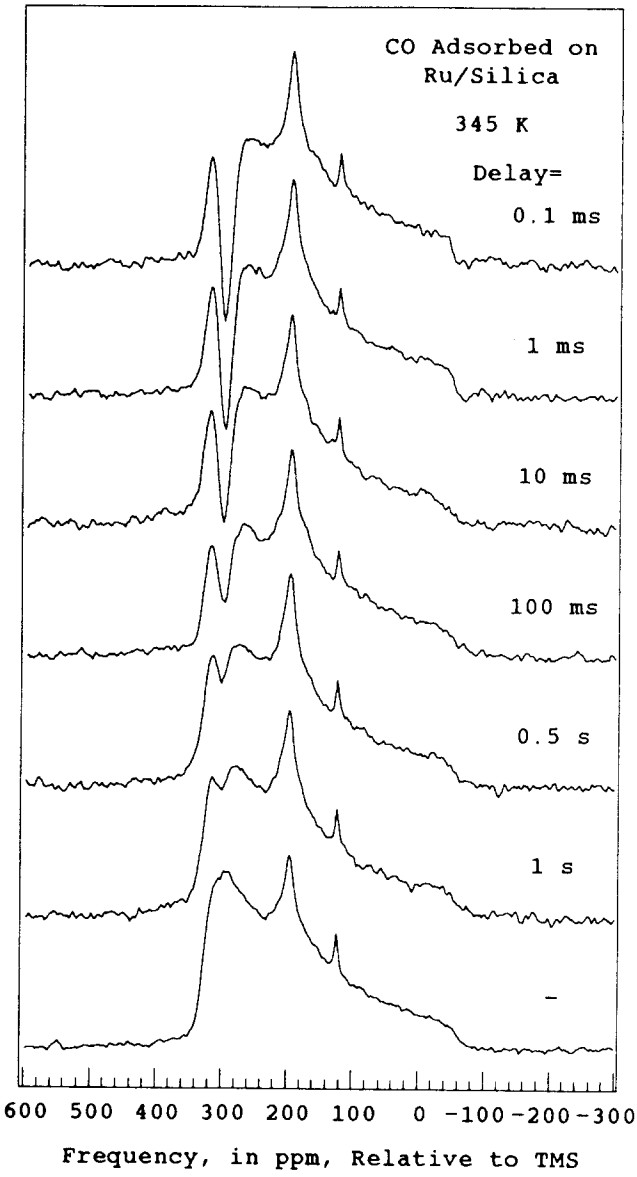

FIG. 3. ^{13}C NMR spectra of CO adsorbed on silica-supported Ru (B) at 345 K as a function of recovery time after selective inversion at 300 ppm. A spectrum measured without inversion is shown at the bottom.

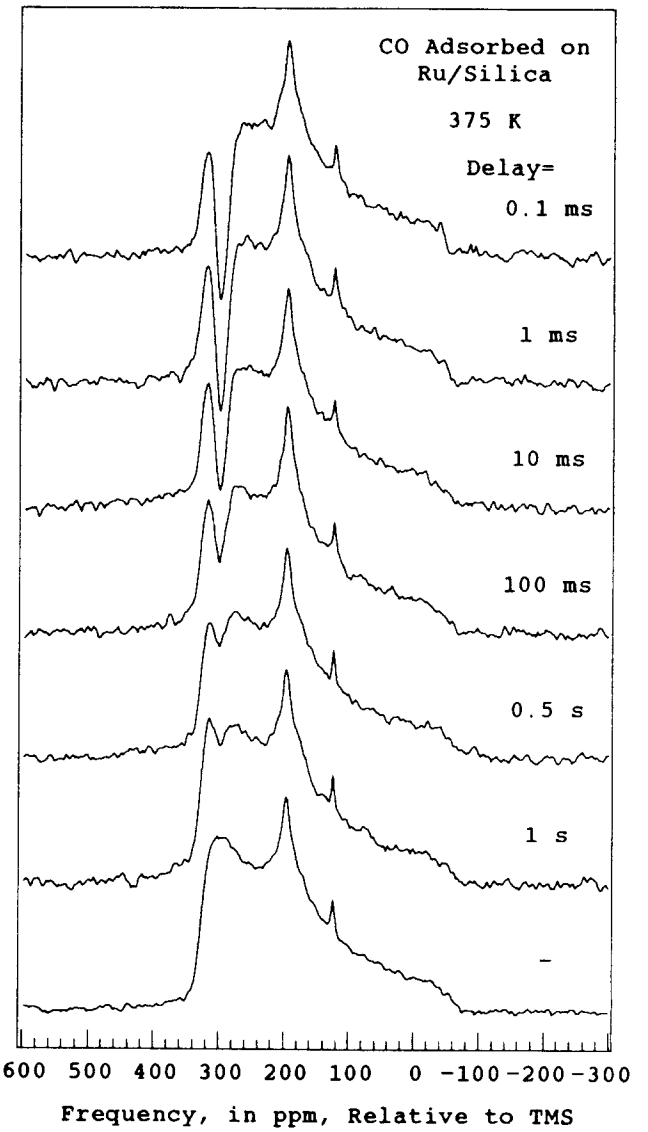

FIG. 4. ^{13}C NMR spectra of CO adsorbed on silica-supported Ru (B) at 375 K as a function of recovery time after selective inversion at 300 ppm. A spectrum measured without inversion is shown at the bottom.

$s_i(\omega)$ is the powder pattern for component i, obtained by convoluting the theoretical expression for g-tensor shielding,[9,10] $I_i(\omega)$, with a Lorentzian broadening function of half-width $\Delta\omega$,

$$s_i(\omega) = \frac{1}{\pi\Delta\omega}\int_{-\infty}^{\infty} \frac{I_i(\omega)}{1+(\omega-\omega')^2/(\Delta\omega)^2}d\omega' \qquad (2)$$

Explicit formulas for $I_i(\omega)$ are given, for example, in the monograph by Haeberlen.[9] A position within a powder pattern, relative to the position of an arbitrary standard, is given by

$$\omega = \omega_0[\langle\sigma\rangle - \tfrac{1}{2}\delta((3\cos^2\theta - 1) + \eta\sin^2\theta\cos 2\phi)]. \qquad (3)$$

The angles θ and ϕ specify the orientation of the CO principal axis system relative to H_0; for CO parallel to H_0, $\theta = 0$. The NMR parameters $\langle\sigma\rangle$, δ, and η, which are the isotropic shift, shielding anisotropy and asymmetry, respectively, are given in Table I for the ^{13}C NMR powder patterns of the various CO species. For linearly bonded CO and, for example, threefold bridged CO, η is zero and there is a one-to-one correspondence between the polar angle θ and the frequency ω. From Eq. (3) one can determine the change in ω caused by a change in orientation (θ, ϕ) or chemical transformation $(\langle\sigma\rangle, \delta, \eta)$. The aggregate change in ω is reflected by the change in the NMR spectrum. For the more general case of nonaxial symmetry ($\eta \neq 0$), one may also determine the effects of changes in orientation and bonding, although the analysis is more complicated. That is, selective irradiation at a particular frequency still labels an orientationally distinct subgroup of the species, but now the subgroup is a function of *both* θ and ϕ. As illustrated in Ref. 9, isochromats for $\eta = 0$ correspond to circles on the unit sphere, whereas for $\eta \neq 0$ the isochromats are eccentric. The complications of $\eta \neq 0$ can be minimized by irradiating near the principal component farthest from the isotropic shift.

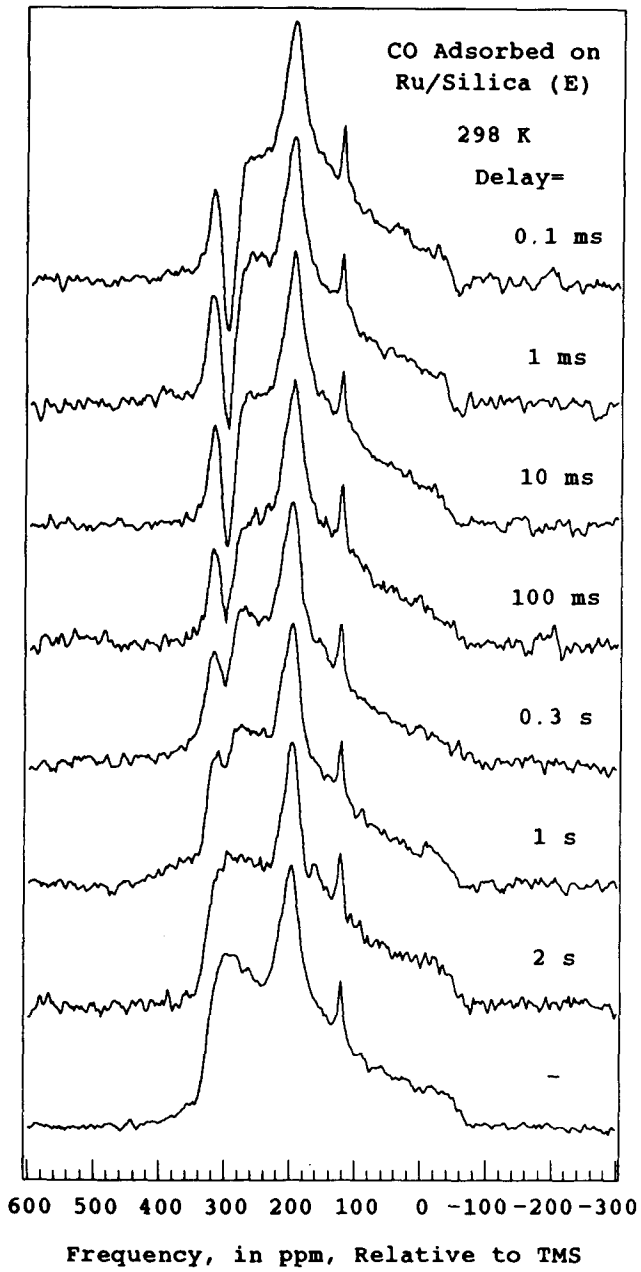

FIG. 5. ^{13}C NMR spectra of CO adsorbed on silica-supported Ru (E) at 298 K as a function of recovery time after selective inversion at 300 ppm. A spectrum measured without inversion is shown at the bottom.

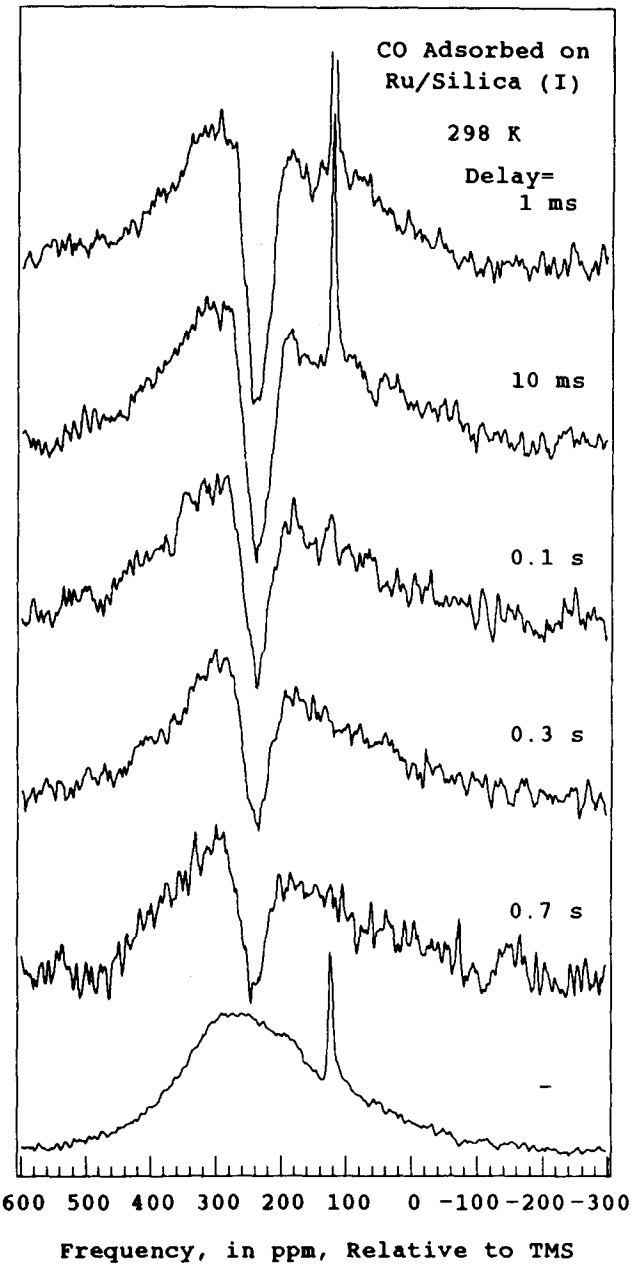

FIG. 6. ^{13}C NMR spectra of CO adsorbed on silica-supported Ru (I) at 298 K as a function of recovery time after selective inversion at 235 ppm. These spectra were acquired with a single-pulse inversion. A spectrum measured without inversion is shown at the bottom.

A spectrum observed at time τ_{rec} after the system is irradiated with the labeling pulse may be represented as

$$S(\omega,\tau_{rec}) = \sum_{i=1}^{n} w_i s_i(\omega)\left[1 - h_i(\omega,\tau_{rec})e^{-\tau_{rec}/T_{1,i}}\right], \quad (4)$$

where $T_{1,i}$ is the spin-lattice relaxation time constant for species i and $h_i(\omega,\tau_{rec})$ is the profile of the spectral hole, the nonequilibrium magnetization. Immediately after irradiation with the inversion sequence shown in Fig. 1, the spin-population hole profile is a Gaussian centered at ω_h, with amplitude A_0, such that $0 \leqslant A_0 \leqslant 1$, and half-width $\Delta\omega_h$, as given by

$$h_i(\omega,0) = 2A_0 \exp\left[\frac{-(\omega-\omega_h)^2}{2(\Delta\omega_h)^2}\right]. \quad (5)$$

If a weak 180° pulse of duration t_p is used, the initial hole profile is that given by[2]

$$h_i(\omega,0) = A_0\left\{\frac{1-\cos[\pi(1+\xi^2)^{1/2}]}{1+\xi^2}\right\}, \quad (6)$$

such that

$$\xi = \frac{1}{\pi}(\omega-\omega_h)t_p. \quad (7)$$

The goal of the following sections is to obtain expressions for

$h_i(\omega,\tau_{rec})$ for a given motional process. The processes for CO on metal particles considered here are desorption to (or exchange with) the gas phase and surface diffusion. Site exchange (e.g., linearly bonded to bridged-bonded) is discussed elsewhere[11] and, because in this study both the linear and bridged CO on a surface are labeled, it is not a relevant process.

1. Desorption and exchange with gas-phase CO

Thermally activated desorption of CO may be described with first-order kinetics. Because the spectrum of $CO(g)$ is not observed, desorption will not create a hole elsewhere in the observed spectrum and the hole profile is given by

$$h_i(\omega,\tau_{rec}) = e^{-\tau_{rec}/\tau_{des}} h_i(\omega,0). \tag{8}$$

The temperature dependence of the desorption time constant τ_{des} is[12]

$$\tau_{des} = \tau_0 \exp\left(\frac{E_{des}}{kT}\right). \tag{9}$$

The prefactor τ_0 is typically $10^{-14\pm2}$ s and the heat of adsorption E_{des} for CO on Ru(001) is $\sim$26 kcal/mol at high coverage.[13] Thus, τ_{des} is $\sim 10^6$ s at 298 K and $\sim 10^3$ s at 375 K, much longer than the lifetime of the NMR spin labels ($T_1 \approx 1$ s) and thus not detectable in this study.

Although thermal desorption is too slow to be observed here, desorption stimulated by adsorption from the gas phase may be much faster. For example, although E_{des} is about 32 kcal/mol for CO on Rh(111), $^{13}CO_{ads}$ on Rh particles exchanges with $^{12}CO_g$ in a few seconds at 50 Torr and >250 K.[14] For CO on Ni(100), the presence of gas-phase CO can shift E_{des} to 9.7 kcal/mol from 26.7 kcal/mol for thermal desorption.[15] The time constant for CO on Pd was found to have the functional form given by[16]

$$\tau^*_{des} = \frac{\tau^*_0}{P^n} \exp\left(\frac{E^*_{des}}{kT}\right). \tag{10}$$

This formula was derived from data in the range $339 \leqslant T \leqslant 466$ K and $10^{-8} \leqslant P \leqslant 10^{-7}$ Torr, which suggested $\tau^*_0 \approx 10^{-8}$ s Torr^{-1}, $n \approx 0.79$, and $E^*_{des} \approx 4.9$ kcal/mol.

2. Surface diffusion

Surface diffusion due to a concentration gradient can be modeled with Fick's second law,

$$\frac{\partial C}{\partial t} = D\nabla^2 C, \tag{11}$$

where C is the concentration of nonequilibrium population of the ^{13}C spin polarization and D is the surface diffusion coefficient, assumed to be independent of position. The concentration as a function of ω is the difference between the labeled and unlabeled spectra, which from Eqs. (1) and (4) is

$$C(\omega,\tau_{rec}) = \sum_i w_i c_i(\omega,\tau_{rec}), \tag{12}$$

$$c_i(\omega,\tau_{rec}) = h_i(\omega,\tau_{rec}) s_i(\omega) e^{-\tau_{rec}/T_{1,i}}. \tag{13}$$

The surface diffusion coefficient is a function of temperature, as given by

$$D = D_0 \exp\left[\frac{-E_{act,dif}(T_r - T)}{kTT_r}\right], \tag{14}$$

such that D_0 is the diffusion coefficient at reference temperature T_r. All measurements here are at saturation coverage and thus the coverage dependence of D is not included.

Diffusion about the surface of a particle will be revealed by the evolution of the labeled NMR spectra if the diffusion changes the orientation of the CO bond. Thus, diffusion about a flat surface will have no effect on the NMR spectra; the hole will relax with rate T_1. (Albeit, T_1 may be shorter than that of immobile adsorbed CO.) We consider here two other particle shapes for which surface diffusion will change the CO orientation: spheres (or half spheres) and multifaceted particles.

(a) *Multifaceted particles.* We calculate here the diffusion between a labeled surface and adjoining unlabeled surfaces. For this diffusion to cause a change in the NMR spectrum, the change in Larmor frequency that accompanies diffusion to an adjoining surface must be larger than the baseline width of the spectral hole, which is about 35 ppm in this study. Thus, from Eq. (3) the relative angles between the surface normals of adjacent surfaces must be larger than 10°. We approximate this system by considering diffusion between a labeled rectangular surface ($2l_x \times 2l_y$) to four adjacent, semi-infinite surfaces. Thus, the system can be projected onto a two-dimensional coordinate system. The concentration of spin labels as a function of (x,y) measured from the center of the labeled surface is obtained from Fick's second law for diffusion as expressed by

$$\frac{\partial C}{\partial t} = D\left(\frac{\partial^2 C}{\partial x^2} + \frac{\partial^2 C}{\partial y^2}\right), \tag{15}$$

such that

$$C(t=0) = \begin{cases} C_0 & \text{(labeled surface)} \\ 0 & \text{(neighboring surface).} \end{cases} \tag{16}$$

The solution to Eq. (15) with initial conditions (16) is[17,18]

$$C(x,y,t) = \frac{1}{4} C_0 \left\{\mathrm{erf}\left[\frac{l_x - x}{2(Dt)^{1/2}}\right] + \mathrm{erf}\left[\frac{l_x + x}{2(Dt)^{1/2}}\right]\right\} \times \left\{\mathrm{erf}\left[\frac{l_y - y}{2(Dt)^{1/2}}\right] + \mathrm{erf}\left[\frac{l_y + y}{2(Dt)^{1/2}}\right]\right\}. \tag{17}$$

The two assumptions that the adjoining surfaces are semi-infinite and unconnected by additional surfaces may cause the model to be inaccurate at times long relative to l^2/D, although the two assumptions are somewhat mutually compensating.

If the adjoining surfaces lie at arbitrary angles relative to the labeled surface, diffusion between surfaces moves the nonequilibrium magnetization to arbitrary positions in the powder pattern. Therefore, new holes formed by diffusion will be spread across the entire powder pattern, and thus no discrete holes will appear as the initial hole recovers, as is observed. However, even if the Ru particles are uniform polyhedra it is unlikely that new holes will be observed, as follows. For a labeled surface with its normal at angle θ_1 relative to H_0, diffusion to adjacent surfaces with normals lying at a relative angle θ_2 will move the labeled magnetization to an orientation in the range $\theta_1 + \theta_2$ to $|\theta_1 - \theta_2|$. Thus, the

new hole may be quite broad and would be unlikely to be observed unless the labeled surface had a normal near 0°. The position of the hole in the present studies precludes the appearance of distinct new holes, even if the particles are regular polyhedra.

We will concentrate on the recovery of the original hole. To get an expression for the time dependence of the profile of the original hole in the spectrum, we integrate over the labeled surface:

$$h(\omega,\tau_{\rm rec}) = \left[\frac{1}{l_x l_y}\int_{-l_y}^{l_y}\int_{-l_x}^{l_x} c(x,y,\tau_{\rm rec})\,dx\,dy\right] h(\omega,0) \quad \text{for } (\omega_h - 2\Delta\omega_h) \lesssim \omega \lesssim (\omega_h + 2\Delta\omega_h). \tag{18}$$

Equation (17) applies for the case where the four adjoining surfaces are unlabeled, which is not the case for labeling near $\sigma_\perp$. Some surfaces with normals near $\sigma_\perp$ will also have edges parallel ($\pm 3°$) to H_0 ($\sim 3\%$ of the surfaces), and thus two of the adjoining surfaces will be labeled the same as the center surface. In this case the last multiplicand in Eq. (17) is dropped.

It is possible that diffusion over the surface edges is much slower than diffusion within a flat area. In this limit the concentration of labeled spins on the flat surfaces is uniform as the system equilibrates; the only gradients are at the edges. From Fick's first law the concentration on the labeled surface decreases exponentially and Eq. (17) is replaced by

$$C(x<l_x, y<l_y, t) = C_0 e^{-t/\tau_{\rm edge}}. \tag{19}$$

$\tau_{\rm edge}$ is the time constant for an admolecule adsorbed at the edge to cross over the edge. This model again assumes that the surrounding unlabeled areas are much larger than the labeled area so that the concentration essentially approaches zero.

(b) *Spheres.* In addition to the normal definition, for this model a sphere may also be a particle with many flat surfaces. However, the relative angle between the surface normals of adjacent surfaces must be smaller than the width of the hole (10° in this study). For metal clusters with less than ~ 200 atoms the angular change for a single-site exchange is larger than 10°, and thus these clusters are not spheres in this model. Because of the symmetry of the problem, half spheres give the same result. To model surface diffusion on a sphere of radius r, Fick's law is most conveniently expressed in polar coordinates:

$$\frac{\partial C}{\partial t} = \frac{D}{r^2}\left[\frac{1}{\sin\theta}\frac{\partial}{\partial\theta}\left(\sin\theta\frac{\partial C}{\partial\theta}\right) + \frac{1}{\sin^2\theta}\frac{\partial^2 C}{\partial\phi^2}\right]. \tag{20}$$

We assume D is uniform over the surface of the sphere. The dependence on ϕ vanishes for axially symmetric shielding, as is the case for linearly bonded CO. We will also use this approximation for bridged CO and drop this term from Eq. (20). The general solution to (20) is given in Eq. (21), where P_n is a Legendre polynomial of order n:

$$C(\cos\theta,t) = \sum_{n=0}^{\infty} k_n e^{-n(n+1)\frac{Dt}{r^2}} P_n(\cos\theta). \tag{21}$$

The coefficients k_n are calculated by numerical integration with the initial profile, $h_i(\omega,0)$, and Eq. (3) with $\eta = 0$:[19]

$$k_n = (n+\tfrac{1}{2})\int_0^{\pi} P_n(\cos\theta) \times \exp\left\{\frac{-\delta^2(P_2(\cos\theta) - P_2(\cos\theta_h))^2}{2[\Delta P_2(\cos\theta_h)]^2}\right\} d\cos\theta. \tag{22}$$

For the selective excitation used here, in which the half-width of the hole [$\Delta\omega_h = \Delta P_2(\cos\theta_h)$] is $\sim 0.04\delta$, a representation of the Gaussian hole with less than 0.1% deviation is attained with $n = 80$ near $\sigma_\perp$. Near $\theta = 90°$, $P_n(\cos\theta)$ decreases rapidly with n and thus the first few terms dominate the sum in Eq. (21). Consequently, the recovery of a hole near $\sigma_\perp$ is nearly exponential.

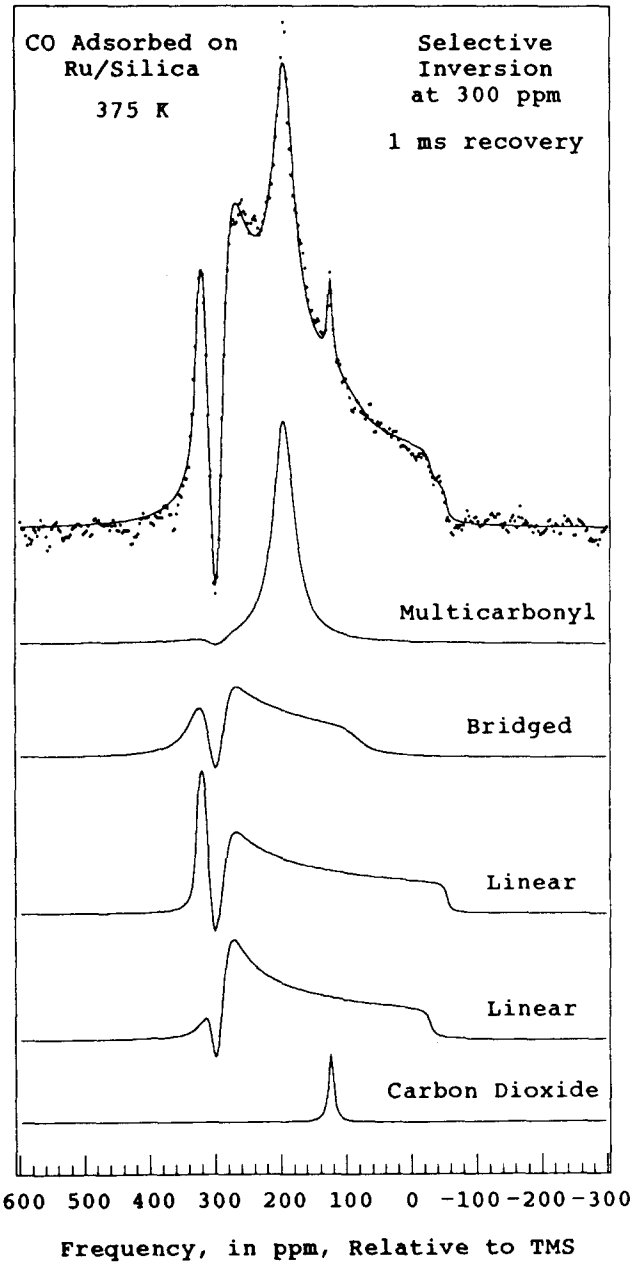

FIG. 7. A four-component fit (plus CO_2) to the ^{13}C NMR spectrum of CO on Ru/silica (B) measured at 375 K, 1 ms after a selective inversion pulse at 300 ppm.

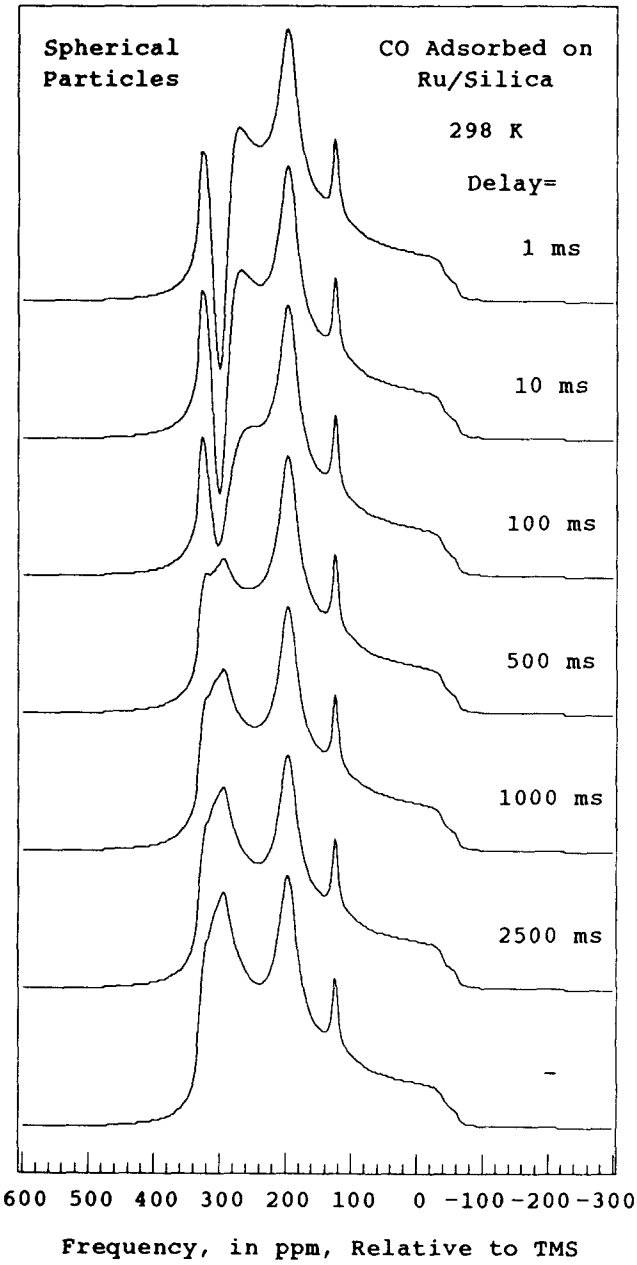

FIG. 8. Simulated spectra calculated for diffusion on a sphere for Ru/silica (B) at 298 K with a hole at 300 ppm. These spectra were calculated with $D/r^2 = 0.018\ s^{-1}$.

3. Combined effect of multiple motions

The evolution of a labeled spectrum of a system undergoing multiple motional processes is immediately available with the formalism developed here. The result is given by Eq. (4) such that h_i is the product of the applicable h_i's derived for the various processes.

B. Analysis of spectra

For a given temperature and hole position, the labeled spectra are analyzed by comparison to the unlabeled spectrum. We employ two techniques which produce consistent results but differ by a factor of $\sim 10^3$ in computation time. In the first method, the unlabeled spectrum is fit with a sum of line shapes corresponding to the individual components, using Eqs. (1–3), which yields the parameters given in Table I, as described elsewhere.[4–7] The labeled spectra are then fit with the composite line shape mulitiplied by the hole profile as expressed in Eq. (4). For example, in those cases where the profile remains Gaussian as the hole recovers, each fit involves the optimization of only two parameters: the amplitude and width of the Gaussian. The chemical shielding parameters and weight fractions determined by fitting the unlabeled spectrum are not varied. This method has the advantage of showing the effect of the labeling on each component as shown in the representative fit plotted in Fig. 7. The second, faster method is a more direct comparison; the unlabeled spectrum is subtracted from each labeled spectrum revealing the nonequilibrium magnetization. The difference spectrum is then directly fit to an expression for a hole profile, $h(\omega,\tau_{rec})$.

Analysis of the spectra in Figs. 2–6 reveals that the hole profile retains its original shape and width throughout its recovery. This is inconsistent with the spherical particle which predicts broadening of the hole as it recovers. Also, the rate of recovery of the hole predicted by the spherical-particle model does not agree with the observed spectra. Whereas the holes are observed to recover over ~ 2 decades, the spherical-particle model predicts a more sudden recovery which is partly an illusion caused by rapid broadening of the hole after it is about one-half recovered. As an example, spectra simulated using the spherical-particle model for Ru/silica (B) at 298 K with the hole at 300 ppm (Fig. 2) are shown in Fig. 8.

Since the hole maintains its original shape, we may decide between the remaining models by examining the time dependence of the amplitude. Figures 9 and 10 contain plots of the integrated hole intensity vs the recovery time. Also included in each plot is the predicted rate if recovery were

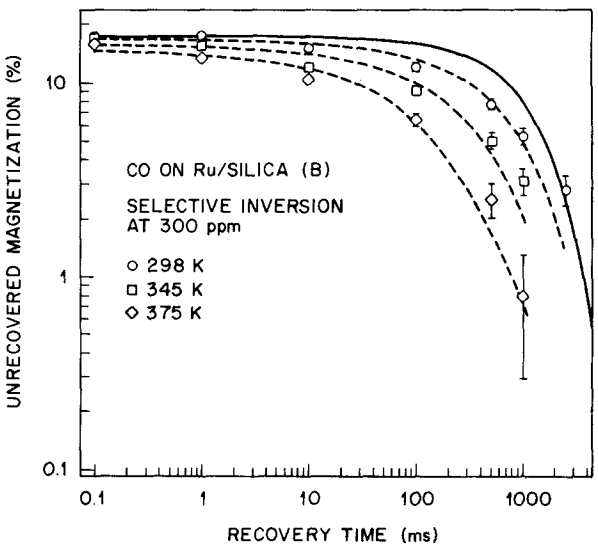

FIG. 9. The fraction of unrecovered magnetization as a function of recovery time for ^{13}C NMR spectra of CO on Ru/silica (B), with selective inversion at 300 ppm, at three temperatures. The solid line is the T_1 relaxation limit at 298 K. The dashed lines are the decays predicted by surface diffusion on multifaceted particles.

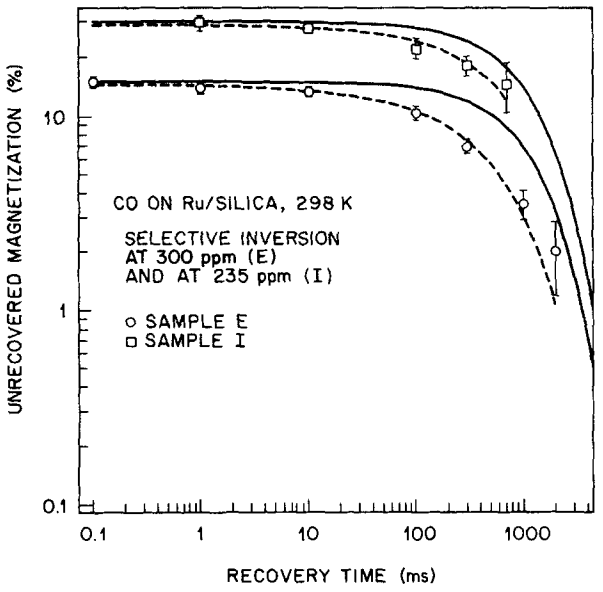

FIG. 10. The fraction of unrecovered magnetization as a function of recovery time for ^{13}C NMR spectra of CO on Ru/silica (E) and (I) at 298 K. The solid lines are the T_1 relaxation limits at 298 K. The dashed lines are the decays predicted by surface diffusion on multifaceted particles.

entirely caused by spin-lattice relaxation. These reference lines serve two purposes: (1) they show that the observed recovery is faster than T_1, and (2) they show the characteristic shape of a single exponential. Clearly, the data in Figs. 9 and 10 do not exhibit exponential recovery. This rules out desorption, surface-gas exchange, and the model in which diffusion over an edge is rate limiting. The stimulated-desorption model is also inconsistent with the relative rates on Ru/silica samples (B) and (E); P_{CO} in (E) is 200 times less but the recovery is slightly faster. Thus, we conclude that the recovery of the hole in a spectrum is caused by surface diffusion on multifaceted particles.

The results of fitting the recovery data to the model for surface diffusion on multifaceted particles are shown by the dashed lines in Figs. 9 and 10. The parameters derived from the fits are given in Table II. The temperature dependence of the characteristic diffusion rate, D/l^2, yields the activation energy of 5.4 kcal/mol for surface diffusion of CO on Ru/silica. This is in good agreement with a measurement on single-crystal Ru. Using laser-induced thermal desorption (LITD), the macroscopic diffusion of CO on Ru(001) at $\theta = 0.58$ was found to have an activation energy of 6.2 kcal/mol.[20] Furthermore, it was observed that the activation energy decreases as CO coverage increases,[20] so extrapolation of their results may lead to even better agreement. However, this agreement is perhaps better than should be expected, given the following differences. First, the substrate studied with LITD is one face of a crystal, whereas supported Ru particles may not be single crystals and have several different surfaces. Second, different diffusion processes are measured in the two experiments. In LITD, diffusion is a vacancy-mediated process driven by a gradient in the CO surface density. At the CO pressures in the NMR samples, the particles have essentially no vacancies and the process is self-diffusion of labeled adsorbates at uniform adsorbate surface density. We note that the uniformity of the surface density of an adsorbate during NMR measurement provides a means to directly measure the diffusion coefficient at a single coverage, in contrast to techniques like LITD which measure diffusion by creating a gradient in the adsorbate surface density and thus measure an averaged D.

TABLE II. Diffusion coefficients

Sample	Position of hole (ppm)	T (K)	D/l^2 (s^{-1})
Ru/silica (B)	300	298	0.32
		345	1.1
		375	2.2
Ru/silica (E)	300	298	0.5
Ru/silica (I)	235	298	0.12

V. SUMMARY

The surface dynamics of CO on silica-supported Ru particles are probed by spin-population labeling of ^{13}C nuclear magnetic dipoles. The labels are created by narrow-bandwidth pulses which selectively invert ^{13}C nuclear spins on the basis of Larmor frequency. Diffferences in Larmor frequency of adsorbed CO species are chiefly caused by chemical shift anisotropy, and thus the selective inversion labels CO molecules at a specific angle relative to the external magnetic field.

Models for diffusion on spherical and multifaceted particles and for desorption to and exchange with the gas phase are developed to predict the time dependence of the spectral hole. The rate of change of the hole intensity and its constant width suggest the dominant process is surface diffusion on multifaceted particles. The temperature dependence in the range 298–375 K indicates that E_{act} is 5.4 kcal/mol. The invariance of the data measured with samples at two different pressures, 0.5 and 100 Torr, suggests adsorption-assisted exchange with gas-phase CO is not dominant.

ACKNOWLEDGMENTS

The NMR spectroscopy in this paper benefited from numerous discussions and experimental assistance from Dean Douglass. We received suggestions from John Yates, Jr. and John Gland on adsorption-assisted desorption, from Steve George on coverage-dependent diffusion, and from Eric Shaqfeh on the mathematical models.

[1] S. E. Shore, J.-Ph. Ansermet, C. P. Slichter, and J. H. Sinfelt, Phys. Rev. Lett. **58**, 953 (1987).
[2] T. W. Root and T. M. Duncan, J. Catal. **102**, 109 (1986).
[3] T. W. Root and T. M. Duncan, Chem. Phys. Lett. **137**, 57 (1987).
[4] T. M. Duncan and T. W. Root, J. Phys. Chem. **92**, 4426 (1988).
[5] T. M. Duncan, K. W. Zilm, D. M. Hamilton, and T. W. Root, J. Phys. Chem. **94**, 2583 (1989).
[6] A. M. Thayer, T. M. Duncan, and D. C. Douglass, J. Phys. Chem. (in press).
[7] T. M. Duncan, P. Winslow, and A. T. Bell, J. Catal. **93**, 1 (1985).
[8] (a) J. Friedrich, S. Davies, and R. Freeman, J. Magn. Reson. **75**, 390 (1987); (b) V. Sklenár, L. Pucek, R. Fiala, and Z. Starcuk (personal com-

munication).
[9]U. Haeberlen, *High Resolution NMR in Solids—Selective Averaging; Advances in Magnetic Resonance, Supplement 1.* (Academic, New York, 1976).
[10]N. Bloembergen and J. A. Rowland, Acta Metall. **1**, 731 (1953).
[11]T. M. Duncan, A. M. Thayer, and T. W. Root, Phys. Rev. Lett. **63**, 62 (1989).
[12]A. Clark, *The Theory of Adsorption and Catalysis* (Academic, New York, 1970).
[13]H. Pfnur, P. Feulner, H. A. Engelhardt, and D. Menzel, Chem. Phys. Lett. **59**, 481 (1978).
[14]J. T. Yates, Jr., T. M. Duncan, and R. W. Vaughan, J. Chem. Phys. **71**, 3908 (1979).
[15]J. T. Yates, Jr. and D. W. Goodman, J. Chem. Phys. **73**, 5371 (1980).
[16]T. Yamada, T. Onishi, and K. Tamaru, J. Chem. Phys. **33**, 533 (1983).
[17]J. Crank, *The Mathematics of Diffusion*, 2nd ed. (Oxford University, New York, 1975).
[18]H. S. Carslaw and J. C. Jaeger, *Conduction of Heat in Solids* (Clarendon, Oxford, 1959).
[19]E. D. Rainville, *Special Functions* (McMillan, New York, 1960).
[20]A. A. Deckert, J. L. Brand, M. V. Arena, and S. M. George, Surf. Sci. **208**, 441 (1989).